Thermodynamics and phase diagrams of lead-free solder materials

H. Ipser · H. Flandorfer · Ch. Luef · C. Schmetterer · U. Saeed

Published online: 14 September 2006

Abstract Many of the existing and most promising lead-free solders for electronics contain tin or tin and indium as a low melting base alloy with small additions of silver and/or copper. Layers of nickel or palladium are frequently used contact materials. This makes the two quaternary systems Ag–Cu–Ni–Sn and Ag–In–Pd–Sn of considerable importance for the understanding of the processes that occur during soldering and during operation of the soldered devices. The present review gives a brief survey on experimental thermodynamic and phase diagram research in our laboratory. Thermodynamic data were obtained by calorimetric measurements, whereas phase equilibria were determined by X-ray diffraction, thermal analyses and metallographic methods (optical and electron microscopy). Enthalpies of mixing for liquid alloys are reported for the binary systems Ag–Sn, Cu–Sn, Ni–Sn, In–Sn, Pd–Sn, and Ag–Ni, the ternary systems Ag–Cu–Sn, Cu–Ni–Sn, Ag–Ni–Sn, Ag–Pd–Sn, In–Pd–Sn, and Ag–In–Sn, and the two quaternary systems themselves, i.e. Ag–Cu–Ni–Sn, and Ag–In–Pd–Sn. Enthalpies of formation are given for solid intermetallic compounds in the three systems Ag–Sn, Cu–Sn, and Ni–Sn. Phase equilibria are presented for binary Ni–Sn and ternary Ag–Ni–Sn, Ag–In–Pd and In–Pd–Sn. In addition, enthalpies of mixing of liquid alloys are also reported for the two ternary systems Bi–Cu–Sn and Bi–Sn–Zn which are of interest for Bi–Sn and Sn–Zn solders.

H. Ipser (✉) · H. Flandorfer · Ch. Luef · C. Schmetterer · U. Saeed
Institut für Anorganische Chemie/Materialchemie, Universität Wien, Währingerstrasse 42, A-1090 Wien, Austria
e-mail: herbert.ipser@univie.ac.at

1 Introduction

Joining by soldering in electronics can be considered as a three step procedure:

- Melting of the solder alloy
- Contacting and solidification
- Aging of the solder joint during operation

The melting and solidification behavior as well as the interfacial reactions occurring during soldering and during operation highly influence the soldering process and the performance and durability of solder joints. Eutectic structures and solid solutions are without doubt necessary for a good soldered joint to form but the role of the intermetallics that are formed is somewhat ambivalent. According to [1], the formation of a thin layer of intermetallic compounds is absolutely necessary, however, the formation of thick layers of intermetallic compounds is frequently detrimental to the properties of the joint. As intermetallic compounds are usually brittle, they may be the cause for cracks in a particular solder joint and, as a consequence, be responsible for failure of the entire electronic part.

For a comprehensive understanding of all these processes information on the phase equilibria in the intermetallic systems generated by soldering are indispensable, and this should be supported by the relevant information on thermodynamic properties. Lead-free solders are binary but often also ternary or higher-order alloys, and together with one or more contact materials this results in multi-component systems. Any experimental study of such multi-component systems is tedious and time consuming but the

well-known CALPHAD procedure (see for example Ref. [2] and references therein) provides a possible way to calculate—or extrapolate—phase equilibria in such systems based on reliable binary and ternary data. This reduces the experimental effort considerably since only a limited number of well planned key experiments will be necessary.

Many of the existing and most promising lead-free solders for electronics contain Sn or Sn and In as a low melting base alloy with small additions of Ag and/or Cu, whereas layers of Ni or Pd are frequently used contact materials. This makes the two quaternary systems Ag–Cu–Ni–Sn and Ag–In–Pd–Sn of considerable importance for the understanding of the processes that occur during soldering and during operation of the soldered devices. Thus the major aim of our series of investigations was the determination of thermodynamic properties and phase equilibria in these systems as well as in several of the binary and ternary subsystems. This should provide the basis for CALPHAD-type optimizations as part of a Thermodynamic Database [3]. Thermodynamic measurements included enthalpies of mixing, $\Delta_{mix}H$, of liquid alloys in the quaternaries themselves and in most of the constituent ternaries. Binary liquid alloys were only investigated where literature data were contradictory or incomplete. Extended calorimetric investigations at different temperatures were performed for liquid Ag–Sn, Cu–Sn, and Ni–Sn alloys since noticeable temperature dependencies of the $\Delta_{mix}H$-values had been reported for Ag–Sn and Cu–Sn [4]. In addition, enthalpies of formation, $\Delta_f H$, of solid intermetallic compounds in the systems Ag–Sn, Cu–Sn, and Ni–Sn were determined by tin solution calorimetry.

As far as phase equilibria were concerned, literature information was available for all binary subsystems. Therefore, only a few samples were prepared to check for consistency. Especially in one case, in the Ni–Sn system, it was found that the published phase equilibria [5] were obviously not correct and needed a detailed re-investigation. The corresponding phase relations and those in the ternary systems were investigated by means of X-ray diffraction (XRD), thermal analyses (DTA and DSC) and metallography including EDX and EPMA.

Since small additions of Bi and/or Zn are frequently used to adjust an appropriate melting regime of lead-free solder alloys for different applications, an experimental determination of thermochemical data (e.g. the enthalpy of mixing) of relevant ternary systems was started. First results for the ternary systems Cu–Bi–Sn and Bi–Sn–Zn will be presented here.

In this sense, this paper is supposed to give an overview over the series of investigations of thermochemical properties and phase equilibria in our laboratory within the last few years. Table 1 gives a full list of investigated systems together with the references for those cases that have already been published.

2 Literature data

A short literature overview is given for all those systems for which experimental results are reported here that have not yet been published elsewhere. For a detailed overview in all other cases the reader is referred to the corresponding original references (see Table 1).

2.1 Binary systems

2.1.1 Ag–Sn

The system Ag–Sn, now a key system for lead free solder materials, has been extensively studied in the past for various other reasons. Several experimental data sets concerning phase equilibria and thermochemistry are available, with first publications dating back to the end of the 19th century. Thermodynamic evaluations and assessments of the phase diagram including thermochemical data were done by Karakaya and Thompson [15], Chevalier [16] and Xie and Qiao [17]. There is some evidence for a temperature dependence of the enthalpy of mixing of liquid alloys.

Table 1 List of investigated systems together with references

System	Calorimetric measurements	Phase diagram measurements
Ag–Sn	This work	Not investigated
Cu–Sn	This work	Not investigated
Ni–Sn	This work	This work
Pd–Sn	[6]	Not investigated
In–Sn	[6]	Not investigated
Bi–Cu	This work	Not investigated
Ag–Ni	[7]	Not investigated
Ag–Cu–Sn	[8]	Not investigated
Cu–Ni–Sn	[8]	Not investigated
Ag–Ni–Sn	[7]	This work
Ag–Pd–Sn	[9]	Not investigated
In–Pd–Sn	[6]	[10]
Ag–In–Pd	Not investigated	[11, 12]
Bi–Cu–Sn	This work	Not investigated
Bi–Sn–Zn	[13]	Not investigated
Ag–Cu–Ni–Sn	This work	Not investigated
Ag–In–Pd–Sn	[14]	Not investigated

2.1.2 Cu–Sn

Experimental work on this important intermetallic system (brass alloys) has started at the beginning of the 20th century. Extended experimental investigations and a presentation of a phase diagram were published by Raynor [18]. Existing phase diagram versions are mainly based on his work. Thermodynamic evaluations and assessments of the phase diagram including thermochemical data were done by Saunders and Miodownik [19] and Shim et al. [20]. Again, there is evidence for a temperature dependence of the enthalpy of mixing in this system.

2.1.3 Ni–Sn

Comprehensive calorimetric investigations of this system were presented by Haddad et al. [21]. According to these results no significant temperature dependence of the enthalpy of mixing could be observed. Thermal analyses, XRD experiments and metallographic investigations date back to the first half of the 20th century, and the current version of the phase diagram, as assessed by Nash and Nash [5], is mainly based on these data. Further thermodynamic assessments and phase diagram calculations were published by Nash et al. [22] and by Ghosh [23]. Recently, Leineweber et al. [24–26] presented detailed XRD investigations of the various low-temperature modifications of Ni_3Sn_2.

2.1.4 Bi–Cu

Several calorimetric investigations and emf measurements of Bi–Cu alloys can be found in the literature, the first one dating back to 1930. The resulting enthalpies of mixing of liquid alloys are generally endothermic but not always in good agreement with each other. There are two thermodynamic assessments of the Bi–Cu system, from Niemelä et al. [27] and Teppo et al. [28], both of the same research group. The enthalpies of mixing were calculated based on an optimized thermodynamic data set. In general, there is no indication for a significant and systematic temperature dependence of the enthalpies of mixing.

2.2 Ternary systems

2.2.1 Ag–Ni–Sn

Though being one of the constituents of the quaternary Ag–Cu–Ni–Sn key system, literature on the ternary Ag–Ni–Sn system is rather scarce. An experimental isothermal section at 240°C was established by Chen and Hsu [29], whereas calculated isothermal sections are available from Ghosh at 230°C [30] and Chen and Hsu at 240°C [29]. The Sn-rich part of the liquidus projection has been suggested by Chen et al. [31] mainly based on evaluation of primary crystallization fields. Apparently due to experimental difficulties caused by liquid demixing, they made no effort to investigate the (Ag, Ni)-rich part. So far, no ternary compound has been reported in this system.

2.2.2 Bi–Cu–Sn

To the best knowledge of the authors no experimental thermochemical data for the Bi–Cu–Sn ternary system are available from literature.

2.3 Quaternary systems

Experimental data on phase relations in the tin-rich part of Ag–Cu–Ni–Sn, based on the observation of primary crystallization, were published by Chen et al. [32] and Chang et al. [33]. Otherwise, no data are available in the literature for the two quaternary systems Ag–Cu–Ni–Sn and Ag–In–Pd–Sn.

3 Experimental procedures

A very brief and general description of the experimental techniques is given below. For detailed information on sample preparation, heat treatment and specific experimental conditions the reader is referred to the corresponding references [6, 8–14] which are also listed in Table 1 and cited with the different systems in Chapter 4.

3.1 Sample preparation

All samples were synthesized from high purity elements: Ag (shot, 99.98%, ÖGUSSA, Vienna, Austria), heated in a carbon crucible at 700°C for 10 min to remove surface impurities; Bi (pellets, 99.999%, ASARCO, South Plainfield, NJ, USA); In (rod, 99.9999%, ASARCO); Cu (wire, 99.98% Goodfellow, Cambridge, UK), treated under H_2 flow at 150°C for 2 h to remove oxide layers; Ni (sheet, 99.98% Alfa Johnson–Matthey); Pd (sponge, 99.9 %, ÖGUSSA, Vienna, Austria); Sn (rod, 99.9985%); Zn (shot, 99.999%; both Alfa Johnson–Matthey). The Zn was melted under vacuum and filtered through quartz wool for further purification.

3.2 Calorimetric measurements

Calorimetric measurements were carried out in a Calvet-type micro calorimeter (SETARAM, Lyon, France) with a thermopile consisting of more than 200 thermocouples, wire wound resistance furnace, suitable for temperatures up to 1000°C, automatic drop device for up to 30 drops, control and data evaluation with LabView and HiQ as described earlier by [34].

The experimental data were treated by a least squares fit using the Redlich–Kister formalism for the description of substitutional solutions. In the case of ternary alloy systems the so-called Redlich–Kister–Muggiano polynomial was used which takes the additional ternary interactions into account [35, 36]:

$$\Delta H_{\mathrm{mix}}^{\mathrm{tern}} = \sum_i \sum_{j>i} \left[x_i x_j \sum_v L_{i,j}^{(v)} (x_i - x_j)^v \right] + x_i x_j x_k \left(M_{i,j,k}^{(0)} x_i + M_{i,j,k}^{(1)} x_j + M_{i,j,k}^{(2)} x_k \right) \quad (1)$$

The Redlich–Kister–Muggiano formalism can also be extended to describe quaternary systems by the sum of the six binary terms, the four ternary terms and an additional quaternary contribution (see, for example, Fiorani et al. [37]):

$$\Delta H_{\mathrm{mix}}^{\mathrm{quat}} = \sum_i \sum_{j>i} \left[x_i x_j \sum_v L_{i,j}^{(v)} (x_i - x_j)^v \right] + \sum_{i,j,k} P_{i,j,k} x_i x_j x_k + C_{i,j,k,l} x_i x_j x_k x_l \quad (2)$$

where $P_{i,j,k} = x_i\ M_{i,j,k}^{(0)} + x_j\ M_{i,j,k}^{(1)} + x_k\ M_{i,j,k}^{(2)}$ is the ternary contribution and $C_{i,j,k,l}$ is the symmetric quaternary interaction parameter.

3.3 X-ray diffraction

A Guinier–Huber film camera with Cu-$K_{\alpha 1}$ radiation was used to analyze the phase composition of the samples. The powdered samples were fixed on a plastic foil, and pure Si (99,9999%) was used as an internal standard. High Temperature XRD was performed on a Bruker D8 powder diffractometer equipped with an ultra-high speed Vantec 1 detector and with Cu $K_{\alpha 1}$ radiation. The heating device was an Anton Paar HTK 1200N chamber using Ar as inert gas.

3.4 Thermal analyses

Differential Thermal Analysis (DTA) was performed on a Netzsch 404S Thermal Analyzer, equipped with Pt/Pt10%Rh (S-type) thermocouples. Pieces of the samples weighing 200 to 300 mg were used for the DTA measurements. Differential Scanning Calorimetry (DSC) measurements were done on Netzsch 404 DSC equipment using Pt/Pt10%Rh (S-type) thermocouples, with samples weighing between 100 and 150 mg. For increased sensitivity, a few Ni–Sn samples were measured in a Setaram Multi-HTC instrument equipped with a heat-flow DSC transducer using Pt6%Rh/Pt30%Rh (B-type) thermocouples.

3.5 Metallography

Samples to be examined were embedded in a mixture (1:2 volume parts) of Cu Powder and Resinar F (Wirtz/Buehler, Düsseldorf, Germany). This mixture polymerizes by application of pressure and heat yielding a solid block after cooling. Cu is added to obtain a conductive material which is necessary for further investigation by electron microscopy. After embedding the samples were polished first with SiC discs with 600 and 1000 mesh and then with Al_2O_3 (1 μm).

Metallographic investigations were done with a Zeiss Axiotech light microscope with magnifications of 50, 100, 200, 500 and 1000, equipped with a Sony DSC-S75 digital still camera switched to full zoom. If necessary the samples were etched using 1–5% Nital solution (HNO_3 in ethanol) in order to be able to distinguish different phases from each other.

EPMA measurements were carried out on a Cameca SX 100 electron probe using wavelength dispersive spectroscopy (WDS) for quantitative analyses and employing pure elements as standard materials. Conventional ZAF matrix correction was used to calculate the compositions from the measured X-ray intensities.

4 Results and discussion

4.1 Ag–Cu–Ni–Sn and subsystems

4.1.1 Calorimetry

4.1.1.1 Binary systems The integral enthalpies of mixing, $\Delta_{\mathrm{mix}}H$, of liquid binary Ag–Sn, Cu–Sn, and Ni–Sn alloys were determined at different temperatures. The results are presented in Figs. 1–3. The curve fitting procedure and all extrapolations are based on the Redlich–Kister polynomials for substitutional solutions (see Chapter 3.2.); the corresponding interaction parameters, $L^{(v)}$, are listed in Table 2.

All three systems show basically an exothermic mixing behavior with exothermic minima in the Sn-

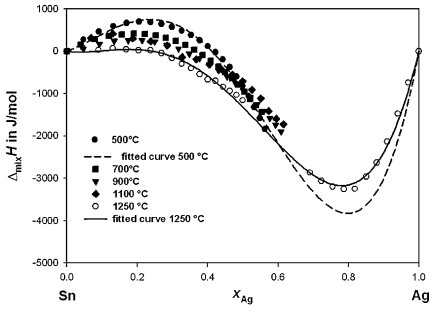

Fig. 1 Integral enthalpy of mixing of liquid Ag–Sn alloys at different temperatures; reference state: Ag(l) and Sn(l)

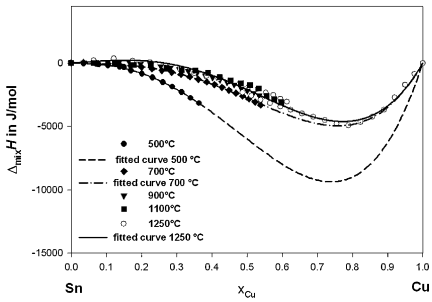

Fig. 2 Integral enthalpy of mixing of liquid Cu–Sn alloys at different temperatures; reference state: Cu(l) and Sn(l)

poor sections. Depending on temperature, the minima are at x_{Ag} = 0.75–0.8 and $\Delta_{mix}H$ = – 3000 to – 4000 J/mol for Ag–Sn, at x_{Cu} = 0.7–0.8 and $\Delta_{mix}H$ = – 4000 to – 9000 J/mol for Cu–Sn, and at x_{Ni}=0.6 and $\Delta_{mix}H$ = – 20000 J/mol for Ni–Sn. These minima correspond nicely to the compositions of the respective most stable solid compounds, Ag_3Sn, Cu_3Sn and Ni_3Sn_2. The minimum values become more negative in the order Ag to Cu to Ni. Additionally, in the case of Ag–Sn and Cu–Sn a significant temperature dependence of these minima was found: the lower the temperature, the lower (i.e. more exothermic) the minimum value. In general, the temperature dependence is significant close to the liquidus and becomes very weak at higher temperatures. These results can be explained according to the association theory for liquid alloys (described in detail by Sommer [38]) by postulating short range ordering in the liquid alloys which is specially pronounced at lower temperatures close to solidification. The compositions of the ''associates'' correspond to the concentrations of the minima of the integral enthalpies of mixing.

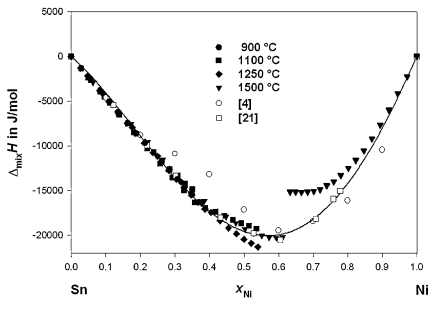

Fig. 3 Integral enthalpy of mixing of liquid Ni–Sn alloys at different temperatures compared with literature data. The solid line shows a fit based on Eq. (1); reference state: Ni(l) and Sn(l)

Whereas $\Delta_{mix}H$ in Ni–Sn is exothermic over the entire concentration range, a slightly endothermic behavior can be observed in the Sn-rich part of Ag–Sn and Cu–Sn. The effect is rather weak in the case of Cu–Sn but more pronounced in Ag–Sn, having a maximum of approx. 800 J/mol at x_{Ag} = 0.3. For a more detailed view on this behavior and especially the temperature dependence of $\Delta_{mix}H$, the limiting partial enthalpies of mixing, $\Delta_{mix}H°$ for Ag, Cu and Ni, respectively, in Sn were determined at 500, 600, 700 and 800°C. All results are presented in Fig. 4, including literature values for Cu in Sn according to Deneuville et al. [39]. As one could expect, the values for Ni in Sn are strongly exothermic, with approx. –60000 J/mol at 500°C. The values show a clear temperature dependence, especially at lower temperatures. Above 800°C the positive temperature coefficient becomes smaller which explains the virtual absence of a significant temperature dependence of $\Delta_{mix}H$ at higher temperatures as seen in Fig. 3.

For Ag in Sn, the partial enthalpy values are positive, with approx. 4300 J/mol at 500°C, showing a very weak negative temperature coefficient.[1] The values for Cu in Sn are slightly positive, approx. 900 J/mol at 500°C, exhibiting a positive temperature coefficient.

The formation of clusters possessing short range order in pure liquid Sn was described by Waseda [40], based on synchrotron X-ray experiments at different temperatures. The clusters disappear at temperatures above 900°C and their structure is similar to that of tetragonal solid Sn, revealing a covalent bonding character. According to the above mentioned association theory Sn-clusters exhibiting a repulsive interaction with

[1] The association theory postulates a positive temperature coefficient of the enthalpy of mixing, but only for systems exhibiting exo- or endo-thermic behavior over the entire concentration range.

Table 2 Interaction parameters in the system Ag–Cu–Ni–Sn

Interaction Parameter	T [°C]	v,α	J/mol
$L^{(v)}_{Ag,Cu}$		0	17396*
		1	2535*
$L^{(v)}_{Ag,Ni}$	1500	0	51381
		1	– 20292
$L^{(v)}_{Ag,Sn}$	500	0	– 2612
		1	– 21559
		2	– 14243
	700	0	– 3719
		1	– 16793
		2	– 10165
	900	0	– 3831
		1	– 15575
		2	– 10888
$L^{(v)}_{Cu,Ni}$	1250	0	14027
		1	– 427
$L^{(v)}_{Cu,Sn}$	500	0	– 23981
		1	– 42563
		2	– 18445
	700	0	– 11093
		1	– 23767
		2	– 13720
	900	0	– 8621
		1	– 21742
		2	– 13128
	1250	0	– 9276
		1	– 24839
		2	– 13346
$L^{(v)}_{Ni,Sn}$	1250	0	– 80939
		1	– 40849
$M^{(\alpha)}_{Ag,Cu,Sn}$	500	0	– 195690
		1	43555
		2	– 27221
	700	0	– 157414
		1	– 164967
		2	– 3843
	900	0	– 127089
		1	– 123769
		2	9929
$M^{(\alpha)}_{Ag,Ni,Sn}$	1000	0	– 235299
		1	– 229480
		2	– 31033
$M^{(\alpha)}_{Cu,Ni,Sn}$	1250	0	– 155990
		1	– 274441
		2	– 19610
$C_{Ag,Cu,Ni,Sn}$	1000		– 471120

* Temperature independent data of different sources

free silver or copper atoms lead to the endothermic enthalpies of mixing.

In the case of additions of Ni to Sn the formation of more stable Ni–Sn associates is favorable. Thus the entire system shows an exothermic enthalpy of mixing.

The enthalpies of formation, $\Delta_f H$ of the binary intermetallic compounds Ag_4Sn, Ag_3Sn, Cu_3Sn (ε-phase), Cu_3Sn (δ-phase), Cu_6Sn_5 (η-phase), Ni_3Sn, Ni_3Sn_2 and Ni_3Sn_4 were obtained from tin solution calorimetry, applying the following equation:

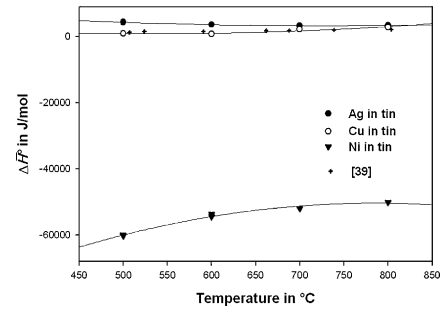

Fig. 4 Partial enthalpies of mixing at infinite dilution for Ag, Cu and Ni in liquid Sn as a function of temperature; reference state: Ag(l), Ni(l) and Cu(l)

$$\Delta_f H^{298} = x \cdot \Delta_{sol}\overline{H}^{\infty}(A) + y \cdot \Delta_{sol}\overline{H}^{\infty}(B) - \Delta_{sol}\overline{H}^{\infty}(A_xB_y) \quad (3)$$

where

- $\Delta_f H^{298}$ is the enthalpy of formation of the intermetallic compounds at 298 K referred to the solid components
- x, y are the mole fractions of the components A and B
- $\Delta_{sol}\overline{H}^{\infty}(A), \Delta_{sol}\overline{H}^{\infty}(B)$, and $\Delta_{sol}\overline{H}^{\infty}(A_xB_y)$ are the limiting enthalpies of dissolution of the solid components in Sn.

All results are summarized in Table 3 including the nominal compositions, heat treatments and a comparison with available literature data.

Figure 5 shows the experimental data of the integral molar enthalpy of mixing for liquid Ag–Ni alloys at 1500°C, measured in several runs from both sides, i.e. starting from pure Ag and pure Ni. As expected for a system with an extended miscibility gap in the liquid, the enthalpy of mixing is positive for all compositions. The curves show a kink at about 4.5 at.% Ni and 1.5 at.% Ag, resp., indicating demixing of the liquid. The extrapolation of fitted experimental values gives a maximum of about 13500 J/mol at approx. 40 at% Ag. Using these results as input into a CALPHAD-type calculation of the binary Ag–Ni phase diagram, the critical temperature of the miscibility gap at 3800 K [49] comes out in good agreement with theoretical calculations of Colinet and Pasturel [50].

4.1.1.2 Ternary Systems Ag–Cu–Sn and Cu–Ni–Sn The original experimental data of the measurement series in the Ag–Cu–Sn system at 500, 700, and

Table 3 Enthalpies of formation of binary intermetallic compounds of Ag–Sn, Cu–Sn and Ni–Sn

Compound	Composition	Annealing temp. [°C]	$\Delta_f H^{298}$ [kJ/mol]	Literature data
Ag_3Sn (ε)	$Ag_{0.744}Sn_{0.256}$	340	–4.18(±1)	–4.5(±0.25)723 K [41]
Ag_4Sn (ζ)	$Ag_{0.848}Sn_{0.152}$	640	–2.82 (±1)	–2.5(±0.25)723 K [41]
				–3.6(±0.10) 723 K [42]
Cu_3Sn (ε)	$Cu_{0.748}Sn_{0.252}$	640	–8.22(±1)	–7.81(±0.2),723K [43]
				–7.53(±0.2), 723K [4]
				–7.82(±0.2), 293 K [44]
				–8.36, 723 K [61]
$Cu_{41}Sn_{11}(\delta)$	$Cu_{0.80}Sn_{0.20}$	700	–5.68(±1)	–5.45(±0.2), 723 K [43]
				–5.46(±0.2), 723 K [4]
Cu_6Sn_5 (η)	$Cu_{0.548}Sn_{0.452}$	200	–6.11 (±1)	–7.03 (±0.05) 273 K [45]
Ni_3Sn (LT)	$Ni_{0.74}Sn_{0.26}$	1050	–24.9 (±1)	–26(±0.5), 1060 K [46]
				–23.4(±4), 298 K [47]
				–23(±0.28), 293 K [4]
Ni_3Sn_2 (HT)	$Ni_{0.577}Sn_{0.423}$	1050	–34.6(±1)	–31(±0.28), 293 K [4]
				–32(±0.5), 1060 K [46]
				–39(±0.2), 1023 K [48]
				–31.3(±4), 298 K [47]
Ni_3Sn_4	$Ni_{0.42}Sn_{0.58}$	600	–24(±1)	–25(±0.5), 1060 K [46]
				–33.7(±0.2), 1023 K [48]

900°C, resp., and in the Cu–Ni–Sn system at 1250°C can be found in Ref. [8]. As the result of a least squares fit, the ternary interaction parameters $M^{(\alpha)}_{Ag:Cu:Sn}$ and $M^{(\alpha)}_{Cu:Ni:Sn}$ were established. All binary and ternary interaction parameters can be found in Table 2.

Based on the Redlich–Kister–Muggiano polynomial (1), iso-enthalpy curves of $\Delta_{mix}H$ in the liquid state were calculated and plotted on Gibbs triangles (see Fig. 6 for Ag–Cu–Sn at 900°C and Fig. 7 for Cu–Ni–Sn at 1250°C). The corresponding analytical functions describe the enthalpy of mixing in the entire system, but it has to be noted that the iso-enthalpy graphs can only be experimentally determined at concentrations where the alloy is completely liquid at the respective temperature. All the other calculated values refer to metastable supercooled liquid alloys. In the graphic representation, the liquidus isotherms from the compilation by Villars et al. [51] were included showing all partially solid regions at the corresponding temperatures shaded in gray.

The Ag–Cu–Sn iso-enthalpy curves are somewhat more complicated than those of Cu–Ni–Sn. With decreasing temperature the enthalpy of mixing of the binary Cu–Sn system becomes significantly more negative. The minimum is situated around the binary Cu_3Sn compound, which is also the global minimum for the Ag–Cu–Sn system (in our fit at $x_{Cu} = 0.74$ and $\Delta_{mix}H = -9.4$ kJ/mol at 500°C, $x_{Cu} = 0.76$ and $\Delta_{mix}H = -5.0$ kJ/mol at 700°C and $x_{Cu} = 0.77$ and $\Delta_{mix}H = -4.3$ kJ/mol at 900°C). A ''valley'' of negative $\Delta_{mix}H$ values runs through the ternary system at around 20 to 30 at.% Sn, connecting the Cu–Sn with the Ag–Sn minimum. The maximum of the fitted surface is positive and appears at the bordering Ag–Cu

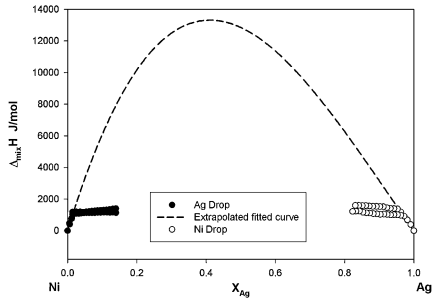

Fig. 5 Integral enthalpy of mixing of liquid Ag–Ni alloys at 1500°C; reference state: Ag (l) and Ni (l)

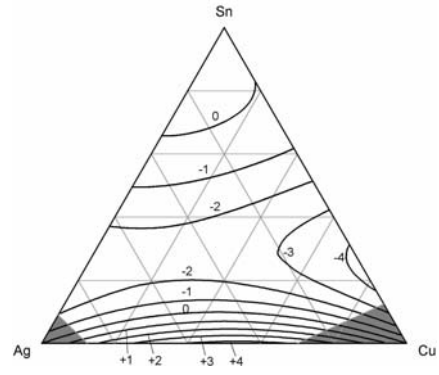

Fig. 6 Integral enthalpy of mixing of liquid Ag–Cu–Sn alloys at 900°C; reference state: Ag(l), Cu(l), Sn(l). Values are in kJ/mol

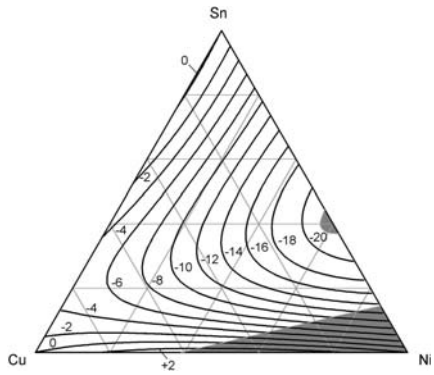

Fig. 7 Integral enthalpy of mixing of liquid Cu–Ni–Sn alloys at 1250°C; reference state: Cu(l), Ni(l), Sn(l). Values are in kJ/mol

binary system. As the temperature decreases, the liquid region in the Ag–Cu–Sn system gets significantly smaller. At 500°C only a small portion in the Sn-rich corner is still liquid, which is the region interesting for lead-free solder materials.

The enthalpy of mixing for the Cu–Ni–Sn system at 1250°C shows a global minimum around the binary Ni_3Sn_2 compound (in our fit at 0 at.% Cu and 60.8 at.% Ni, –21.4 kJ/mol). A ''valley'' runs through the enthalpy surface connecting the binary minima in the Ni–Sn and Cu–Sn system. Next to the binary compound Ni_3Sn_2 and in the Ni-rich corner the system is (partially) solid at this temperature. The maximum of the enthalpy surface is positive and appears along the bordering Cu–Ni binary system, far away from our region of interest for lead-free soldering. Our results for 1250°C are in good agreement with the results for 1307°C by Pool et al. [52].

The enthalpy of mixing of the ternary Ag–Cu–Sn system shows a significant dependence on temperature. The temperature dependence of the ternary interaction parameters $M^{(\alpha)}_{Ag,Cu,Sn}$ is illustrated in Table 2. To obtain a general expression for the value of these parameters as a function of the absolute temperature (in K) they were fitted using a linear polynomial. The results are as follows:

$$M^{(0)}_{Ag,Cu,Sn} = -326936 + 171.50 \cdot T$$
$$M^{(1)}_{Ag,Cu,Sn} = -365395 + 205.99 \cdot T$$
$$M^{(2)}_{Ag,Cu,Sn} = -97412 + 92.88 \cdot T$$

Note that for the temperature dependence of the parameter $M^{(1)}$ only the values for 700 and 900°C were considered since its value at 500°C deviates considerably from the linear trend and would require a much more complicated equation. Therefore the equations given above should only be used to calculate the ternary interaction parameters for temperatures above 700°C, for lower temperatures the dependence might be more complicated. With the combined results it is now possible to calculate the enthalpy of mixing of liquid Ag–Cu–Sn alloys for any desired ternary concentration at different temperatures.

4.1.1.3 Ternary system Ag–Ni–Sn In the ternary Ag–Ni–Sn system the enthalpies of mixing were determined at 1000, 1220 and 1400°C. In one series of experiments, pieces of pure Ni (20 to 40 mg) were dropped into approx. 1 g of molten Ag–Sn alloys (10, 20, 30, 70, 80, and 90 at.% Sn), in another series, pure Ag was added to liquid Ni–Sn alloys (10, 20, 30, 70, 80, and 90 at.% Sn). From the composition dependence of the integral enthalpy values and from the constant values of the partial enthalpy, the concentration limits of the homogeneous liquid phase and the type of the second phase segregating from the liquid could be deduced. It was either the primary crystallization of solid Ni_3Sn_2 or the appearance of a second liquid phase due to the extension of the liquid miscibility gap in the ternary system. All these results are presented in Fig. 8.

Applying the polynomial described above, isoenthalpy curves for liquid ternary Ag–Ni–Sn mixtures at 1000°C are presented in Fig. 9. As in the other

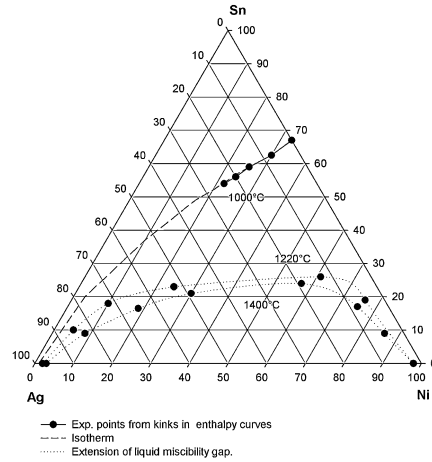

Fig. 8 Extension of the homogeneous liquid phase in the Ag–Ni–Sn system at 1000°C (liquidus), 1220 and 1400°C (liquid miscibility gap) from calorimetric measurement

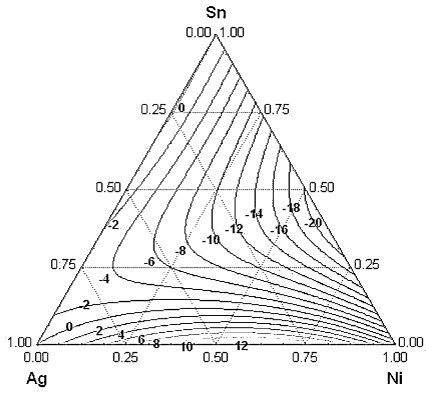

Fig. 9 Integral enthalpy of mixing of liquid Ag–Ni–Sn alloys at 1000°C; reference state: Ag(l), Ni(l), Sn(l). Values are in kJ/mol

ternary systems, the plot refers to the metastable liquid phase for all those compositions where the alloy is not completely liquid at 1000°C.

It can be seen that $\Delta_{mix}H$ is mostly negative except in the region close to the Ag–Ni binary (where one can find the global endothermic maximum of 13.5 kJ/mol) and in the narrow region close to the Sn-rich part of the Ag–Sn binary system. The enthalpy of mixing shows a minimum of – 20 kJ/mol corresponding to the binary minimum of Ni–Sn around 60 at.% Ni.

4.1.1.4 Quaternary System Ag–Cu–Ni–Sn In the quaternary Ag–Cu–Ni–Sn system, the enthalpies of mixing were determined at 1000°C along nine sections. Starting with ternary Ag–Cu–Sn alloys ($0.4 \leq x_{Sn} \leq 0.9$) in the crucible, 15 to 18 drops of pure nickel were added for each section. Figures 10 and 11 show,

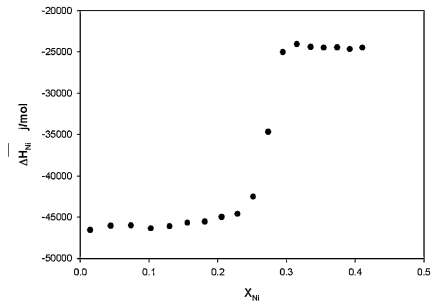

Fig. 11 Partial enthalpy of mixing of Ni in quaternary liquid Ag–Cu–Ni–Sn alloys along a section starting from $Ag_5Cu_5Sn_{90}$ at 1000°C; reference state: Ag(l), Cu(l), Ni(l), Sn(l)

as an example, the integral and partial liquid enthalpies of mixing along one section, starting from $Ag_5Cu_5Sn_{90}$, in the quaternary Ag–Cu–Ni–Sn system at 1000°C. It can be seen that the $\Delta_{mix}H$ curve in Fig. 10 shows a kink at approx. 28 at.% Ni which corresponds to a jump in the partial enthalpy to a constant value of approx. –25000 J/mol (Fig. 11). This is caused by the primary crystallization of a solid phase, most probably Ni_3Sn_2. Similar behavior was found in all other investigated sections.

The experimental enthalpies of mixing of the quaternary Ag–Cu–Ni–Sn alloys were fitted based on Eq. (2) (see Chapter 3.2). All the necessary binary and ternary interaction parameter can be found in Table 2. Following Luo et al. [53], the term for the ternary interactions in Ag–Cu–Ni was skipped assuming ideal mixing of the binary liquid alloys.

Usually, from a statistical point of view, the contribution of quaternary interactions to the overall enthalpy of mixing is expected to be small. Indeed, the

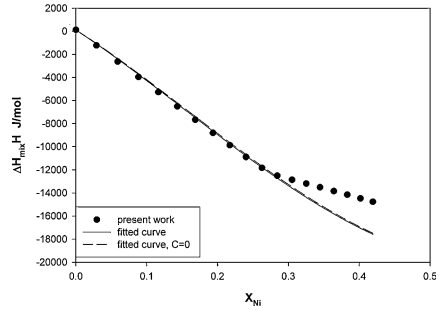

Fig. 10 Integral enthalpy of mixing of quaternary liquid Ag–Cu–Ni–Sn alloys along a section starting from ternary $Ag_5Cu_5Sn_{90}$ at 1000°C; reference state Ag(l), Cu(l), Ni(l), Sn(l)

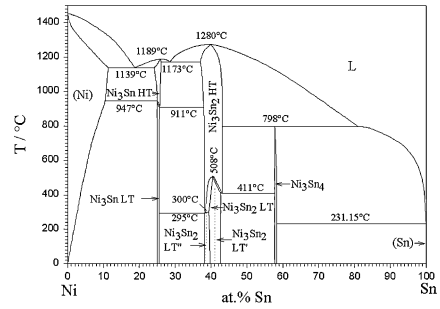

Fig. 12 Ni–Sn phase diagram revised according to the results of the present investigation, including data from Leineweber et al. [24–26]

resulting symmetric quaternary interaction parameter of $C_{Ag,Cu,Ni,Sn} = -471120$ J/mol is relatively small, considering that it has to be multiplied by a factor $x_{Ag} \cdot x_{Cu} \cdot x_{Ni} \cdot x_{Sn}$: it gives a maximum contribution of 1840 J/mol to the integral enthalpy at $x_{Ag} = x_{Cu} = x_{Ni} = x_{Sn}$. In Fig. 10 the experimental values of a quaternary section are compared with the calculated curve including $C_{Ag,Cu,Ni,Sn}$ (solid line) and without quaternary interaction (dashed line). Considering the estimated errors of these calorimetric techniques it is clear that $C_{Ag,Cu,Ni,Sn}$ can be neglected, as has been shown recently for the general case by Fiorani et al. [37].

4.1.2 Phase diagrams

4.1.2.1 Ni–Sn A new version of the Ni–Sn phase diagram was established based on thermal analyses, XRD techniques and EPMA on samples annealed at various temperatures. Homogeneity ranges of intermetallic phases and reaction temperatures were modified according to our results.

The crystal structure of the HT-Ni_3Sn phase was found to be cubic (BiF_3 type) using high temperature XRD. This phase either undergoes martensitic transformation to a β-Cu_3Ti structure on quenching at very high cooling rates or a massive transformation to the hexagonal LT-Ni_3Sn phase. The phase transition was found to comprise a peritectoid and a eutectoid reaction at 947 and 911°C, resp., which is in contrast to the available literature [5]. Furthermore, the Ni_3Sn_2 region was considerably modified: two incommensurate Ni_3Sn_2 low temperature phases (LT′ and LT″), first reported by Leineweber et al. [24–26], were included as well as the rather complicated transition to the Ni_3Sn_2 HT-phase. Figure 12 shows the modified Ni–Sn phase diagram according to our results.

4.1.2.2 Ag–Ni–Sn This ternary system is dominated by a liquid miscibility gap which extends from the binary Ag–Ni system into the ternary up to about 35 at.% Sn. No ternary intermetallic compound has been found in this system so far, and the binary phases have very limited or negligible ternary solubilities. Isothermal sections at 200, 450, 700 and 1050°C were established based on results of EPMA and XRD for more than 120 ternary samples prepared by different methods and annealed at several temperatures. As an example, the isothermal section at 450°C is shown in Fig. 13. The liquidus was estimated from thermal analysis and metallography. Certain phase fields involving the various modifications of Ni_3Sn_2 have not been clarified yet because of the complexity of the

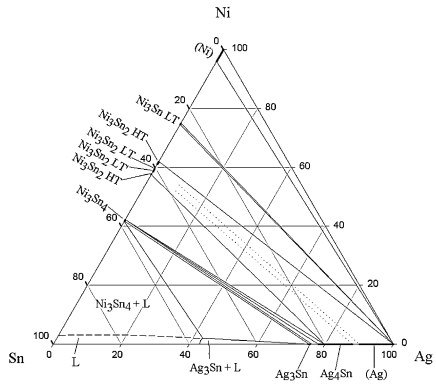

Fig. 13 Isothermal section of the Ag–Ni–Sn phase diagram at 450°C

involved phase transitions; any phase boundaries are therefore represented by dotted lines.

The tentative liquidus projection shown in Fig. 14 was deduced from results of thermal analyses. According to our experiments, the invariant reaction U2 was placed at $Ag_{64}Ni_1Sn_{35}$ and at a temperature of 570°C which is in contrast to previous work by Chen et al. [31]. All invariant reactions are listed in Table 4. The (Ag,Ni)-rich part of the liquidus projection remains still somewhat unclear because of severe experimental difficulties in that area.

4.2 Ag–In–Pd–Sn and subsystems

4.2.1 Calorimetry

The original experimental data of the measurement series in the ternary systems In–Pd–Sn and Ag–Pd–Sn,

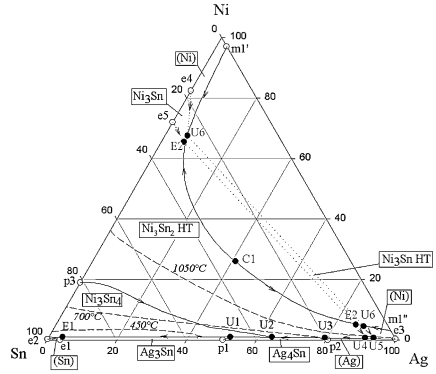

Fig. 14 Liquidus projection of Ag–Ni–Sn phase diagram; fields of primary crystallization are indicated

Table 4 Invariant reactions in the system Ag–Ni–Sn

Reaction	Type	Temperature [°C]	
		This work	Chen et al. [31]
L → (Sn) + Ni_3Sn_4 + Ag_3Sn	E1	220	219
L + Ag_4Sn → Ni_3Sn_4 + Ag_3Sn	U1	485	488
L + Ni_3Sn_2 → Ag_4Sn + Ni_3Sn_4	U2	570	516.5
L + (Ag) → Ag_4Sn + Ni_3Sn_2 HT	U3	725	
L2 + Ni_3Sn HT → Ni_3Sn_2 HT + (Ag)	U4	Unknown	
L2 + (Ni) → Ni_3Sn HT + (Ag)	U5	Unknown	
L1 → L2 + Ni_3Sn HT + Ni_3Sn_2 HT	E2	1130	
L1 + (Ni) → L2 + Ni_3Sn HT	U6	~1135	
Critical point	C1	1130 < T < 1270	

and the quaternary system Ag–In–Pd–Sn can be found in Refs. [6, 9, 14], respectively. All quaternary measurements were performed at 900°C. The $\Delta_{mix}H$ values of the ternary liquid alloys were again fitted employing Eq. (1). Binary and ternary interaction parameters are listed in Table 5.

The resulting iso-enthalpy plots for In–Pd–Sn and Ag–Pd–Sn are shown in Figs. 15 and 16, respectively. In the diagrams, the estimated course of the liquidus isotherm at 900°C is included, showing all regions shaded in gray where the system is not totally liquid.

Table 5 Interaction parameters in the system Ag–In–Pd–Sn

Interaction Parameter	T [°C]	ν,α	J/mol
$L^{(\nu)}_{Ag,In}$	1000	0	– 15443
		1	– 12728
		2	3844
$L^{(\nu)}_{Ag,Pd}$	1400	0	– 19141
		1	– 15925
$L^{(\nu)}_{Ag,Sn}$	500	0	– 2612
		1	– 21559
		2	– 14243
	700	0	– 3719
		1	– 16793
		2	– 10165
	900	0	– 3831
		1	– 15575
		2	– 10888
$L^{(\nu)}_{In,Pd}$	900	0	– 202640
		1	85610
$L^{(\nu)}_{In,Sn}$	900	0	– 1481
		1	– 499
$L^{(\nu)}_{Pd,Sn}$	900	0	– 215814
		1	– 126046
$M^{(\alpha)}_{Ag,In,Pd}$	938	0	– 275878
		1	66245
		2	– 653632
$M^{(\alpha)}_{Ag,In,Sn}$	727–980	0	32696
		1	44749
		2	10393
$M^{(\alpha)}_{Ag,Pd,Sn}$	900	0	– 313084
		1	– 422417
		2	113838
$M^{(\alpha)}_{In,Pd,Sn}$	900	0	156065
		1	253787
		2	211126
$C_{Ag,In,Pd,Sn}$	900		351260

It can be seen that the enthalpy of mixing in the In–Pd–Sn system is negative over the entire composition range and shows a global minimum of –57.0 kJ/mol on the binary Pd–Sn edge at 56 at.% Pd. In the Ag–Pd–Sn system the enthalpy of mixing is negative almost over the entire composition range, except for a very small region along the Sn-rich part of the binary Ag–Sn where one can find the global endothermic maximum ($\Delta_{mix}H_m$ = + 256 J/mol at 21 at.% Ag). The enthalpy of mixing shows again its minimum of – 57.0 kJ/mol on the binary Pd–Sn edge at 56 at.% Pd.

The experimental integral enthalpy of mixing data in the quaternary system Ag–In–Pd–Sn at 900°C were fitted using Eq. (2), with the necessary interaction parameters taken from Table 5. All those parameters that have been determined at a different temperature were assumed to be temperature independent. Multiplying the resulting value of $C_{Ag,Cu,Ni,Sn}$ = – 351260 J/mol by $x_{Ag} \cdot x_{In} \cdot x_{Pd} \cdot x_{Sn}$ yields a maximum quaternary contribution of 1372 J/mol at $x_{Ag} = x_{In} = x_{Pd} = x_{Sn}$.

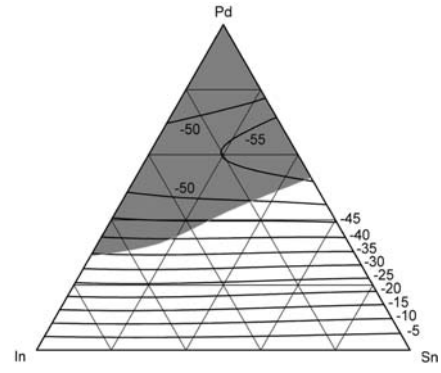

Fig. 15 Integral enthalpy of mixing of liquid In–Pd–Sn alloys at 900°C; reference state: In(l), Pd(l), Sn(l), values are in kJ/mol

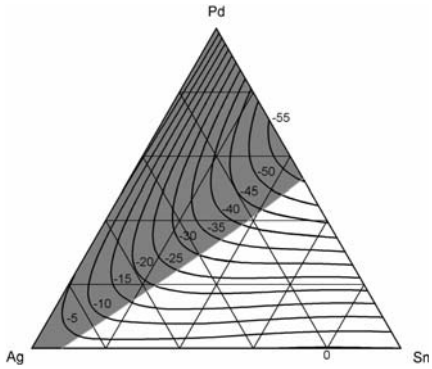

Fig. 16 Integral enthalpy of mixing of liquid Ag–Pd–Sn alloys at 900°C; reference state: Ag(l), Pd(l), Sn(l), values are in kJ/mol

This shows again that, within the experimental uncertainty, this quaternary term can be neglected as in the case of the Ag–Cu–Ni–Sn system (see above).

The enthalpies of mixing of quaternary Ag–In–Pd–Sn alloys at 900°C along one selected section (pure Ag dropped into molten $In_{40}Pd_{20}Sn_{40}$), calculated from Eq. (2), with the interaction parameters from Table 5 and with (solid line) and without (dashed line) $C_{Ag:In:Pd:Sn}$ = 351260 J/mol, are shown in Fig. 17. It can be seen that the measured values are described well by both fits.

4.2.2 Phase diagrams

4.2.2.1 In–Pd–Sn Ternary In–Pd–Sn alloys were synthesized to evaluate the phase relations in that system for Pd contents up to about 60 at.%. The phase compositions of the annealed (180, 500, and 700°C) and quenched samples were characterized by XRD and—for a number of selected samples—also by scanning electron microscopy. The original experimental data can be found in Ref. [10]. Based on binary data from Refs. [54] and [34] and the present results, isothermal sections were constructed for 180, 500, and 700°C.

As an example, the isothermal section at 500°C is presented in Fig. 18. The phase InPd, with an extended homogeneity range in the binary ($0.43 \le x_{In} \le 0.52$), dissolves up to 7 at.% Sn, whereas PdSn was found to dissolve significant amounts of In (approx. 7 at.%); a similar amount of In is dissolved in $Pd_{20}Sn_{13}$. The phase $PdSn_2$ shows an even larger solubility for In: Sn can be substituted by In up to 22 at.% at constant Pd contents. All samples in the composition range below the [In_7Pd_3 + $PdSn_2$] two-phase field were found to be in equilibrium with the liquid. Our results are in general agreement with results of Kosovinc et al. [55, 56] who suggested a continuous solid solubility between the isotypic orthorhombic compounds $\alpha InPd_2$ and Pd_2Sn. Although this has not been proven unambiguously up to now it is in accord with our results.

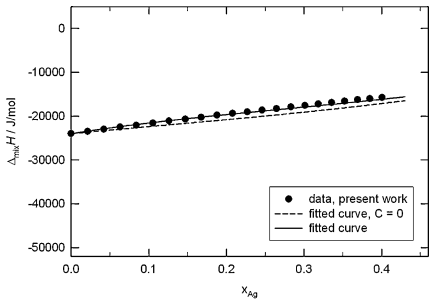

Fig. 17 Integral enthalpy of mixing of quaternary liquid Ag–In–Pd–Sn alloys along a section starting from ternary $In_{40}Pd_{20}Sn_{40}$ at 900°C; reference state: Ag(l), In(l), Pd(l), Sn(l)

4.2.2.2 Ag–In–Pd To obtain a first idea of the phase relationships in the Ag–In–Pd system, a CALPHAD-type calculation was employed and three isothermal sections were calculated at 200, 500, and 700°C, based on optimized versions of the binary systems only, taken from the COST 531 Thermodynamic Data Base [3]. In a next step, the three isothermal sections were investigated experimentally [11, 12] and, as an example, the

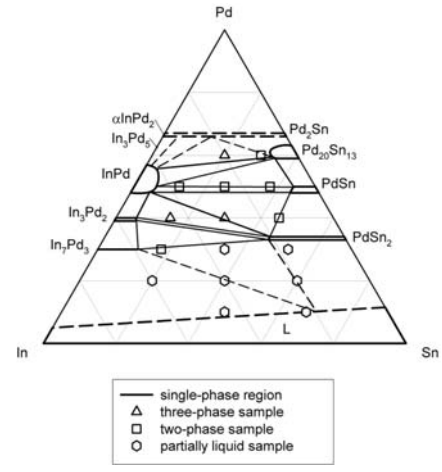

Fig. 18 Isothermal section of In–Pd–Sn phase diagram at 500°C

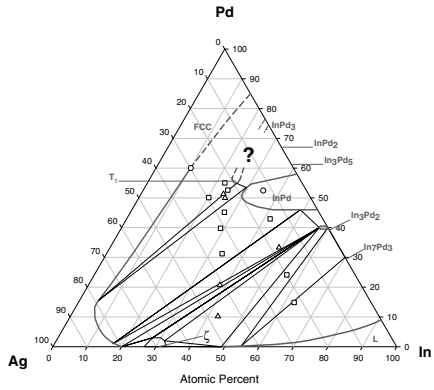

Fig. 19 Phase equilibria in the Ag–In–Pd system at 500°C based on experimental results

section at 500°C is shown in Fig. 19. As can be seen, a ternary compound (T_1) was identified with a crystal structure of the HgMn-type which is related to the structure of the binary compound $InPd_3$ (Al_3Ti type). This structural relationship is probably the reason that its homogeneity range, starting approximately at $Ag_{20}Pd_{55}In_{25}$, extends towards binary $InPd_3$, ending probably around $Ag_{10}Pd_{65}In_{25}$ although the exact position of the two-phase field is still not fully clear.

All experimental phase diagram data were taken together with experimental values for the enthalpy of mixing of liquid Ag–In–Pd alloys [14, 57], and a new CALPHAD optimization of the ternary system was performed [12]. Figure 20 shows the calculated isothermal section at 500°C which can now be compared with the experimental phase diagram in Fig. 19. It can be seen that the agreement is good even if the calculated homogeneity range of InPd is smaller and the ternary phase T_1 is shown as a stoichiometric compound.

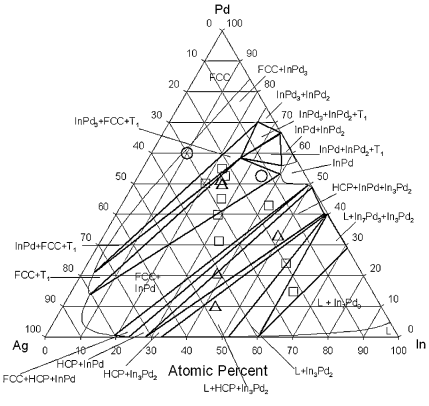

Fig. 20 Phase equilibria in the Ag–In–Pd system at 500°C from a CALPHAD-type calculation and comparison with experimental results: ○, single phase; □, two-phase; Δ, three-phase

4.3 Bi–Cu–Sn

The partial and integral enthalpies of mixing at 800°C of liquid ternary Bi–Cu–Sn alloys were determined along nine sections in a large composition range. Additionally, binary alloys of the constituent system Bi–Cu were investigated at 800 and 1000°C.

For Bi–Cu, the $\Delta_{mix}H$ values are generally positive as expected for this simple eutectic intermetallic system with no mutual solid solubility of the constituents. The maximum value of $\Delta_{mix}H$ at 800°C is approx. 4000 J/mol at $x_{Bi} = 0.55$, whereas the measurements at 1000°C gave a maximum of $\Delta_{mix}H = 5000$ J/mol at $x_{Bi} = 0.50$. This positive temperature coefficient of $\Delta_{mix}H$ is in agreement with the association theory for liquid intermetallic alloys [38].

The integral enthalpy of mixing in the ternary system Bi–Cu–Sn is presented as an iso-enthalpy plot in Fig. 21. It was obtained by fitting our experimental results applying the Redlich–Kister–Muggiano polynomial (Eq. 1). The binary and ternary interaction parameters are listed in Table 6. The minima and maxima of the enthalpy surface correspond to the binary minima and maxima in the systems Cu–Sn and Bi–Cu, resp.

4.4 Bi–Sn–Zn

The original experimental data of the measurement series in the Bi–Sn–Zn system can be found in Luef

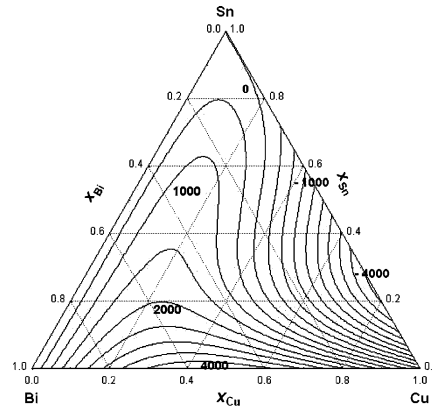

Fig. 21 Integral enthalpy of mixing of liquid Bi–Cu–Sn alloys at 800°C; reference state: Bi(l), Cu(l), Sn(l), values are in J/mol

Table 6 Interaction parameters in the systems Bi–Cu–Sn and Bi–Sn–Zn

Interaction Parameter	T [°C]	ν,α	J/mol
$L^{(\nu)}_{Bi,Sn}$	450	0	442
		1	– 298
$L^{(\nu)}_{Bi,Cu}$	800	0	17810
		1	3331
$L^{(\nu)}_{Cu,Sn}$	800	0	– 9857
		1	– 22755
		2	– 13423
$L^{(\nu)}_{Bi,Zn}$	470–570	0	17782
		1	– 4775
$L^{(\nu)}_{Sn,Zn}$	422–577	0	12558
		1	– 5623
		2	4149
$M^{(\alpha)}_{Bi,Cu,Sn}$	800	0	– 275878
		1	66245
		2	– 653632
$M^{(\alpha)}_{Bi,Sn,Zn}$	500	0	– 15489
		1	– 10785
		2	– 12528

et al. [13]. All measurements were performed at 500°C. Again, the ternary experimental $\Delta_{mix}H$ values of the liquid alloys were fitted by means of Eq. (1), and the obtained binary and ternary interaction parameters are listed in Table 6. Figure 22 shows a corresponding isoenthalpy plot of the integral enthalpy of mixing. The enthalpy of mixing is positive (i.e. endothermic) over the entire composition range. The global maximum of the Bi–Sn–Zn system can be found in the binary Bi–Zn bordering system ($\Delta_{mix}H_m$ = 4523 J/mol at 44 at.% Bi).

Liquidus temperatures and the temperature of the ternary eutectic reaction $E(L \rightleftharpoons (Bi) + (Sn) + (Zn))$ were determined by DSC measurements of 32 samples at constant Zn contents of 3, 5, and 7 at.%, annealed at 150°C. Three different heating rates (10, 5, and 1 K/min) were employed and the thermal effects were linearly extrapolated to zero heating rate. The reaction E was detected in all 32 samples at a temperature of 135.0 ± 0.5°C. This is 5°C higher than the value reported by Muzaffar [58] and also higher than indicated in the recent assessments by Malakhov et al. [59] (126.1°C) and Moelans et al. [60] (131.2°C). From the course of the liquidus temperatures in the three sections it can be estimated that the composition of the liquid in the ternary eutectic reaction is approx. 41 at.% Bi, 57 at.% Sn, and 2 at.% Zn. This is shifted slightly towards lower Zn and higher Sn contents as compared to the values calculated in the two assessments [59, 60].

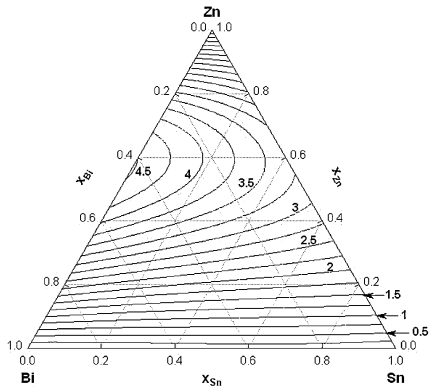

Fig. 22 Integral enthalpy of mixing curves of liquid Bi–Sn–Zn alloys at 500°C; ref. state: Bi(l), Sn(l) and Zn(l); values are in kJ/mol

Acknowledgements The authors acknowledge the financial support of the Austrian ''Fonds zur Förderung der wissenschaftlichen Forschung (FWF)'', projects No. P-15620, P-16495 and P-17346. The financial support of the Hochschuljubilaeumsstiftung der Stadt Wien (Project No. H-812/2005) is also gratefully acknowledged. This research is a contribution to the European COST Action 531 on ''Lead-free Solder Materials''.

References

1. A. Rahn, in *The Basics of Soldering* (John Wiley &Sons Inc., 1993), p. 1
2. Y.A. Chang, S. Chen, F. Zhang, X. Yan, F. Xie, R. Schmid-Fetzer, W.A. Oates, Progr. Mater. Sci. **49**, 313 (2004)
3. A.T. Dinsdale, A. Watson, A. Kroupa, A. Zemanova, J. Vrestal, J. Vizdal, COST 531 Thermodynamic Database, Version 2.0 (2006) (http://www.slihot.co.uk/COST531/td_database.htm)
4. R. Hultgren, P.D. Desai, D. Hawkins, M. Gleiser, K. Kelley, in ''Selected Values of the thermodynamic properties of binary alloys'' (AMS Metals Park, Ohio, 1971)
5. P. Nash, A. Nash, Bull. Alloy Phase Diagrams **6**, 350 (1985)
6. C. Luef, H. Flandorfer, H. Ipser, Thermochim. Acta **417**, 47 (2004)
7. U. Saeed, H. Flandorfer, H. Ipser, J. Mater. Res. **21**, 1294 (2006)
8. C. Luef, H. Flandorfer, H. Ipser, Z. Metallkde. **95**, 151 (2004)
9. C. Luef, A. Paul, H. Flandorfer, A. Kodentsov, H. Ipser, J. Alloys Comp. **391**, 67 (2005)
10. C. Luef, H. Flandorfer, A. Paul, A. Kodentsov, H. Ipser, Intermetallics **13**, 1207 (2005)
11. A. Zemanova, A. Kroupa, J. Vrestal, O. Semenova, K. Chandrasekaran, K.W. Richter, H. Ipser, Monatsh. Chem. **136**, 1931 (2005)
12. A. Zemanova, O. Semenova, A. Kroupa, J. Vrestal, K. Chandrasekaran, K.W. Richter, H. Ipser, Intermetallics, **14**, (2006), in press
13. C. Luef, A. Paul, J. Vizdal, A. Kroupa, A. Kodentsov, H. Ipser, Monatsh. Chem. **137**, 381 (2006)
14. C. Luef, H. Flandorfer, H. Ipser, Metall. Mater. Trans. A **36A**, 1273 (2005)

15. I. Karakaya, W.T. Thompson, Bull. Alloy Phase Diagrams **8**, 340 (1987)
16. P.-Y. Chevalier, Thermochim. Acta **136**, 45 (1988)
17. Y. Xie, Z. Qiao, J. Phase Equil. **17**, 208 (1996)
18. G.-V. Raynor, in *Annotated Equilibrium Diagram Series, No. 2* (The Institute of Metals, London, 1944)
19. N. Saunders, A.P. Miodownik, Bull. Alloy Phase Diagrams **11**, 278 (1990)
20. J.-H. Shim, C.-S. Oh, Z. Metallkde. **87**, 205 (1996)
21. R. Haddad, M. Gaune-Escard, J.-P. Bros, A. Ranninger-Havlicek, E. Hayer, K.L. Komarek, J. Alloys Comp. **247**, 82 (1997)
22. P. Nash, H. Choo, R.B. Schwarz, J. Mat. Sci. **33**, 4949 (1998)
23. G. Ghosh, Metall. Mater. Trans. **30A**, 1481 (1999)
24. A. Leineweber, M. Ellner, E.J. Mittemeijer, J. Solid State Chem. **159**, 191 (2001)
25. A. Leineweber, O. Oeckler, U. Zachwieja, J. Solid State Chem. **177**, 936 (2004)
26. A. Leineweber, J. Solid State Chem. **177**, 1197 (2004)
27. J. Niemelä, G. Effenberg, K. Hack, P. Spencer, CALPHAD **10**, 77 (1986)
28. O. Teppo, J. Niemelä, P. Taskinen, Thermochim. Acta **173**, 137 (1990)
29. S.-W. Chen, H.-F. Hsu, Acta Materialia **52**, 2541 (2004)
30. G. Ghosh, J. Electron. Mater. **29**, 1182 (2000)
31. S.-W. Chen, H.-F. Hsu, Ch.-W. Lin, J. Mater. Res. **19**, 2267 (2004)
32. S.-W. Chen, C.-A. Chang, J. Electr. Mat. **33**, 1071 (2004)
33. C.-A. Chang, S.-W. Chen, C.-N. Chiu, Y.-C. Huang, J. Electr. Mat. **34**, 1135 (2005)
34. H. Flandorfer, J. Alloys Comp. **336**, 176 (2002)
35. I. Ansara, N. Dupin, in *COST 507 Thermochemical database for light metal alloys*, vol. 2 (European Commission DG XII, Luxembourg, 1998) p. 1
36. N. Saunders, A.P. Miodownik, in ''CALPHAD (Calculation of Phase Diagrams): A Comprehensive Guide'' (Pergamon Press, Oxford, UK, 1998)
37. J.M. Fiorani, C. Naguet, J. Hertz, A. Bourkba, L. Bouirden, Z. Metallkde. **88**, 711 (1997)
38. F. Sommer, Z. Metallkde. **73**, 72 (1982)
39. J.-F. Deneuville, C. Chatillon-Colinet, J.-C. Mathieu, E. Bonnier, J. Chim. Phys. **73**, 273 (1976)
40. Y. Waseda, in *The structure of non-crystalline materials* (McGraw-Hill Inc., 1980), p. 56
41. O.J. Kleppa. J. Phys. Chem. **60**, 852 (1956)
42. G.H. Lauri, A.W.H. Morris, J.N. Pratt, Trans. Met. Soc. **236**, 1390 (1966)
43. O.J. Kleppa, Acta Metall. **3**, 255 (1955)
44. J.B. Cohen, J.S Leach, M.B Bever, J. Met. **6**, 1257 (1954)
45. A. Gangulee, G.C. Das, M.B. Bever, Metall. Trans. **4**, 2063 (1973)
46. B. Predel, W. Vogelbein, Thermochim. Acta **30**, 201 (1979)
47. F. Korber, W. Oelsen, Mitt. K. Wilhem Inst. Eisenforsch. Düsseldorf **19**, 209 (1937)
48. H. Dannoehl, H.L. Lukas, Z. Metallkde. **65**, 642 (1974)
49. A. Zemanova, J. Vrestal, A. Kroupa, Research in progress Masaryk University Bruno (2005)
50. C. Colinet, A. Pasturel, Z. Metallkde. **89**, 863 (1998)
51. P. Villars, A. Prince, H. Okamoto, in *Handbook of Ternary Alloy Phase Diagrams* (ASM International, Metals Park, Ohio, 1995)
52. M.J. Pool, I. Arpshofen, B. Predel, E. Schultheiss, Z. Metallkde. **70**, 656 (1979)
53. H.-T. Luo, S. W. Chen, J. Mater. Sci. **31**, 5059 (1996)
54. T.B. Massalski, J.L. Murray, L.H. Bennett, H. Baker, in ''Binary Alloy Phase Diagrams'' (ASM, Materials Park, Ohio, 1990)
55. I. Kosovinc, M. El-Boragy, K. Schubert, Metall **26**, 917 (1972)
56. I. Kosovinc, T. Grgasovic, Rud.-Metal. Zborn. **1**, 71 (1972)
57. E. Hayer, Calorimetrie Analyse Thermique **26**, 262 (1995)
58. S.D. Muzaffar, J. Chem. Soc. **123**, 2341 (1923)
59. D.V. Malakhov, X.J. Liu, I. Ohnuma, K. Ishida, J. Phase Equil. **21**, 514 (2000)
60. N. Moelans, K.C. Hari Kumar, P. Wollants, J. Alloys Comp. **360**, 98 (2003)
61. W. Biltz, W. Wagner, H. Pieper, W. Holverscheit, Z. Anorg. Chem. **134**, 25 (1924)